Microstructure evolution induced by cathodic charging in low temperature carburized 304 austenitic stainless steel

International Journal of Hydrogen Energy 173 (2025) 151357

Contents lists available at ScienceDirect

International Journal of Hydrogen Energy

journal homepage: www.elsevier.com/locate/he

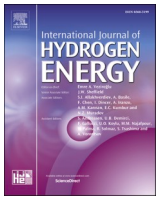

Microstructure evolution induced by cathodic charging in low temperature carburized 304 austenitic stainless steel

Xiao Qin [a,b], Lars Nyborg [a], Huiqun Liu [b], Alexandra Bauer [c], Yu Cao [a,*]

[a] Department of Industrial and Materials Science, Chalmers University of Technology, Gothenburg, 41296, Sweden
[b] School of Materials Science and Engineering, Central South University, Changsha, 410083, PR China
[c] Bodycote Specialist Technologies GmbH, 86899, Landsberg, Germany

ARTICLE INFO

Handling editor: Z Sun

Keywords:
Low-temperature carburizing
Austenitic stainless steel
Hydrogen embrittlement
Expanded austenite

ABSTRACT

This work investigated the effect of hydrogen uptake on the microstructure of low-temperature carburized 304 austenitic stainless steel. Low-temperature carburizing (LTC) treatment introduced a ~22 μm expanded austenite layer with high carbon content and high hardness on the steel surface. Hydrogen was introduced into the steel by cathodic electrochemical charging in an acidic environment. For untreated 304, it was found that hydrogen uptake led to martensitic transformation and orientation-dependent strain. LTC treatment stabilized austenite and suppressed hydrogen-induced martensitic transformation. Surface cracking evolved due to hydrogen uptake. The underlying factors contributing to cracking were discussed. This study revealed that austenite stability and internal stress associated with carbon concentration in expanded austenite were two competing factors affecting cracking resistance. For cold worked 304, LTC treatment significantly reduces hydrogen-induced cracking because the high stability of austenite outweighed the adverse effect of internal stress. However, for solution annealed 304, the high surface carbon concentration introduced by LTC treatment was more dominant, thereby enhancing surface cracking.

1. Introduction

As a sustainable fuel, hydrogen has attracted increasing interest recently due to its potential to significantly reduce greenhouse gas emissions and fossil fuel consumption [1]. However, in applications such as hydrogen fuel vehicles and hydrogen power generation, the safety and durability of structural components are critical concerns. During service, hydrogen can enter the components, causing surface cracking or even premature fracture. In the absence of external stress, surface cracking caused by molecular hydrogen is referred to as hydrogen-induced cracking (HIC). More broadly, premature fracture due to hydrogen, characterized by a loss of strength, toughness and ductility, is known as 'hydrogen embrittlement' (HE), or more generally, 'hydrogen damage' [2–4]. HIC is considered a typical manifestation of HE.

Two primary mechanisms have been proposed to explain HE: hydrogen-enhanced decohesion (HEDE) [3–5] and hydrogen-enhanced localized plasticity (HELP) [6–8]. The HEDE mechanism believes that interstitial hydrogen reduces the cohesive energy within the lattice, at phase boundary or grain boundaries. Specifically, hydrogen atoms occupying the interstitial positions of the metal lattice cause local lattice expansion, which induces internal stress, especially hydrostatic tensile stress, that weakens atomic bonds. Additionally, hydrogen accumulation at grain boundaries or interfaces promotes decohesion and facilitates cracking. Due to current experimental limitations in resolving atomic-scale interactions, the HEDE mechanism is primarily supported by density functional theory simulations [9] and cohesive zone modeling [10]. Fracture surfaces displaying intergranular or cleavage morphologies are typically associated with HEDE. In contrast, the HELP mechanism suggests that hydrogen enhances dislocation activity and localizes plastic deformation. This can result in the formation and coalescence of local microvoids, ultimately leading to crack initiation and propagation. Hydrogen accumulation near crack tips further accelerates localized plastic deformation, contributing to premature failure in the hydrogen-affected zone. Fracture surfaces exhibiting microvoid coalescence and shallow dimples are characteristic of the HELP mechanism.

Austenitic stainless steel (ASS) is widely employed in hydrogen-related applications due to its low hydrogen diffusivity and excellent resistance to HE compared to martensitic and ferritic steels [11–13]. However, its relatively low strength necessitates the use of thicker walls

* Corresponding author.
E-mail address: yu.cao@chalmers.se (Y. Cao).

https://doi.org/10.1016/j.ijhydene.2025.151357
Received 7 March 2025; Received in revised form 1 September 2025; Accepted 2 September 2025
Available online 8 September 2025

in components, leading to increased weight and cost. Strain hardening can be used to improve the strength of ASS, but in metastable grades such as 304 ASS, this process often induces martensitic transformation, which increases the material's sensitivity to HE [14–16]. Therefore, enhancing both the strength and stability of the austenitic phase is essential to broaden the application scope of ASS in hydrogen environments. Carbon, a nickel-equivalent element, plays a dual role. It not only stabilizes the austenite structure but also improves mechanical properties such as hardness and fatigue properties [17]. However, excessive carbon content can lead to carbide precipitation, which seriously compromises corrosion resistance and ductility of ASS. Consequently, effective processing techniques are required to optimize carbon's benefits while preventing the formation of carbides.

In recent years, the technology of low-temperature carburizing (LTC) has attracted widespread attention as a surface treatment technology for ASS. LTC leads to the formation of an interstitial carbon supersaturated austenite layer on the steel surface, commonly referred to as expanded austenite or S-phase [18]. This phase differs from the bulk substrate, as it contains carbon concentrations several orders of magnitude higher than the equilibrium solubility in austenite. The formation of the S-phase significantly enhances the mechanical properties of ASS including hardness, wear resistance, and fatigue properties, while preserving its corrosion resistance [19,20]. Additionally, it has been reported that S-phase improves the resistance of ASS to HE [21,22], However, there is limited understanding of how hydrogen uptake affects the microstructure and stability of the S-phase. Gaining insight into this interaction is crucial for advancing the understanding of HE behavior of the S-phase.

In this study, a commercial ASS, AISI 304, with two different processing conditions (cold worked and solution annealed) was subjected to LTC treatment to obtain expanded austenite on the surface. Hydrogen was introduced into the steel via an electrochemical cathodic charging method, using sulfuric acid solution as the electrolyte. The effect of hydrogen on the microstructure was characterized using a range of techniques, including X-ray diffraction (XRD), scanning electron microscopy (SEM), transmission electron microscopy (TEM) and electron backscatter diffraction (EBSD). This work reveals how LTC affects HIC in 304 ASS from a microstructural aspect.

2. Experimental procedure

The material used in the present work is a commercial AISI 304 ASS with a chemical composition of Fe-0.06C-0.39Si-1.58Mn-18.22Cr-8.02Ni-0.33Cu (wt.%). The as-received samples were cold-drawn bars. For comparison, some bars were solution-annealed at 1050 °C for 1 h and then water quenched. The bars were then machined into discs with a diameter of 10 mm and a thickness of 2 mm for low temperature carburizing and hydrogen charging. Low-temperature carburizing was performed on both cold-worked and solution-annealed 304 by Bodycote using the commercial Kolsterising® K22 process [23] in a carburizing atmosphere at a low temperature (<500 °C) for several days.

Hydrogen charging was performed using electrochemical cathodic method. A platinum mesh electrode was used as the anode, and the sample as the cathode in an aqueous 0.2 mol/L H_2SO_4 solution with 1 g/L Na_2HAsO_4 to avoid recombination of hydrogen. The metallographic samples prepared by mechanical grinding and polishing using OPS (Struers) silica suspension as the final step were charged at a current density of 1–30 mA/cm^2 for 1–24 h at 80 °C. The material conditions in this investigation are summarized in Table 1. LECO ONH-836 hydrogen element analyzer based on inert gas fusion technology was used to measure the total hydrogen content for polished disc samples. After 24 h of hydrogen charging at 80 °C at a current density of 30 mA/cm^2, the samples were stored in a −20 °C refrigerator prior to the measurement. The hydrogen concentration was 10.2 ppm for 304 SA-H and 18 ppm for 304 SA + LTC-H, respectively.

The hardness profiles were obtained on the cross-section of the carburized samples as a function of depth using a DuraScan 70 G5 micro-Vickers hardness tester with a load of 10 gf. The size of the indentation was measured by means of SEM, and the hardness was an averaged value from five points. The metallographic structure of the carburized samples was examined by an optical microscope (OM, ZEISS Axioscope 7, Germany) after etching with V2A reagent (120 ml HCl + 12 ml HNO_3 + 120 ml H_2O). The microstructure was also studied by scanning electron microscope (SEM) and electron backscatter diffraction (EBSD) using a LEO Gemini 1550 FE-SEM coupled with an Oxford Nordlys collection system. In order to study the effect of hydrogen uptake on the microstructure, quasi-in-situ SEM and EBSD were performed before and after hydrogen charging at the same location. Vickers hardness indentation was used for navigation. The step size of EBSD map acquisition was 0.1 μm. The accelerating voltage was set at 20 kV and the working distance was about 14 mm. HKL* Channel 5 data analysis software was used for inverse pole figure (IPF), grain boundary (GB), image quality (IQ), kernel average misorientation (KAM) maps, and phase analysis. Electron channel contrast imaging (ECCI) was performed on a Zeiss-Gemini 450 FE-SEM using a BSE detector to observe crystal defects. An electron probe micro analyzer (EPMA, JEOL JXA-8230) was used to measure carbon concentrations along the depth of the carburized layer. The phases were identified by X-ray diffraction technique, using a Bruker D8 Discover diffractometer equipped with Cu-radiation operated at a voltage of 40 kV and a current of 40 mA. All samples for XRD characterization were polished with 1 μm diamond suspension to ensure the same testing conditions. To study the effect of hydrogen charging on the dislocation density of 304 ASS, thin films in a thickness of about 100 μm were low temperature carburized followed by hydrogen charging and polishing using a dual-jet electropolisher (Struers, TenuPol-5, Denmark) in an electrolyte containing perchloric acid and methanol (1:9) at temperatures below – 30 °C and a voltage range of 30 V. A FEI Tecnai F30 transmission electron microscopy (TEM) with a voltage of 300 kV was used to observe dislocations.

Table 1
Samples used in this study.

Name of samples	Conditions
304 CW	Cold-worked 304
304 SA	Solution-annealed 304
304 CW-H	Cold-worked 304 charged with hydrogen
304 SA-H	Solution-annealed 304 charged with hydrogen
304 CW + LTC	Carburized cold-worked 304
304 SA + LTC	Carburized solution-annealed 304
304 CW + LTC-H	Carburized cold-worked 304 followed by hydrogen charging
304 SA + LTC-H	Carburized solution-annealed 304 followed by hydrogen charging

3. Results

3.1. Characteristics of low-temperature carburized layer

Fig. 1 displays optical micrographs of cross-section taken from carburized 304 coupons. A continuous and clearly distinguishable carburized layer (expanded austenite γ_c) with a thickness of ~22 μm was observed on the steel surface. Compared to the substrate, these carburized layers appeared featureless, indicating improved corrosion resistance against V2A reagents. This agrees well with the literature [18,19]. In the cold-worked sample, slip bands were found within the grains. In some cases, these extended into the expanded austenite layer. By contrast, the solution annealed sample showed twins without slip bands. In both conditions, pits originating from inclusion stripping were detected. The thickness of the expanded austenite layer was comparable between cold-worked and solution-annealed samples, indicating an insignificant effect of processing conditions on layer formation.

Carbon content and Vickers microhardness as a function of depth for LTC-treated samples are shown in Fig. 2. Both decreased gradually with increasing depth until reaching a stable plateau. Interestingly, compared

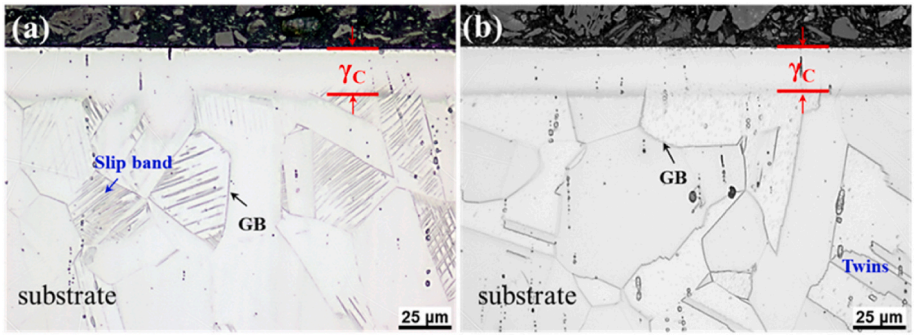

Fig. 1. Light-optical micrographs of the low-temperature carburized specimens after etching in V2A: (a) cold worked and (b) solution annealed 304.

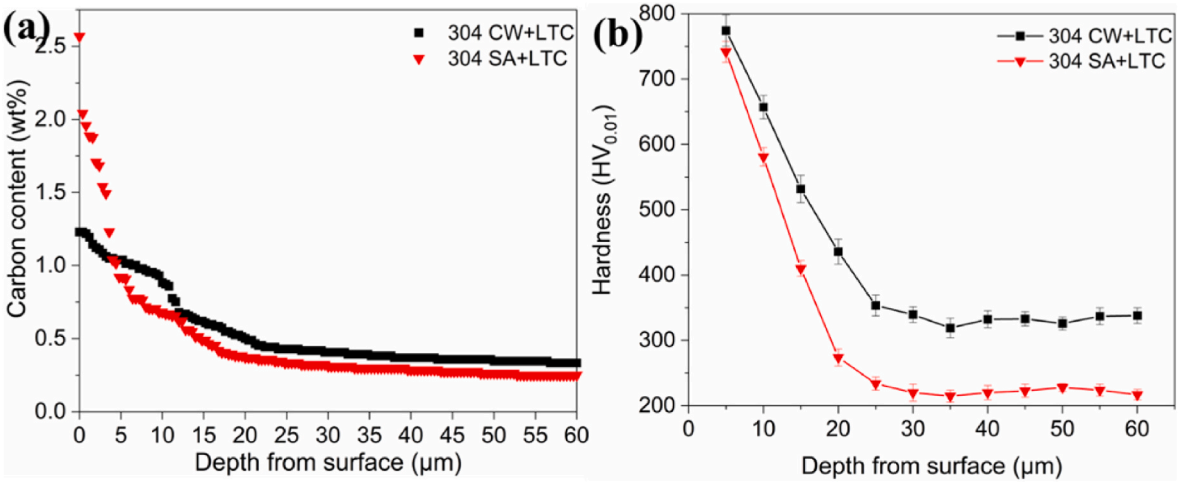

Fig. 2. Carbon concentration (a) and Vickers hardness (b) as a function of depth for the carburized 304 specimens.

to 304 SA + LTC, a significantly lower C-uptake (~1.25 vs 2.5 wt%) was observed at the surface of 304 CW + LTC. This difference can be rationalized by considering the effects of cold working on metastable 304 stainless steel. For metastable 304, cold deformation promotes (i) the formation of deformation induced martensite with bcc/bct structure, and (ii) the introduction of a high density of lattice defects. Together, these features enhance the inward diffusion of carbon during subsequent LTC treatment compared to solution annealed 304 having a fully austenite structure. The resulting carbon profile in 304 CW + LTC is therefore less steep, with a lower surface concentration but deeper penetration. When the depth was larger than ~5 μm, the carbon concentration in 304 CW + LTC sample exceeds that of 304 SA + LTC.

The near surface γ_C layer exhibited extremely high hardness (~775 HV for 304 CW + LTC and ~740 HV for 304 SA + LTC) compared with the underlying substrate (~350 HV for 304 CW and ~220 HV for 304 SA). The gradual decrease in hardness with depth correlated with the

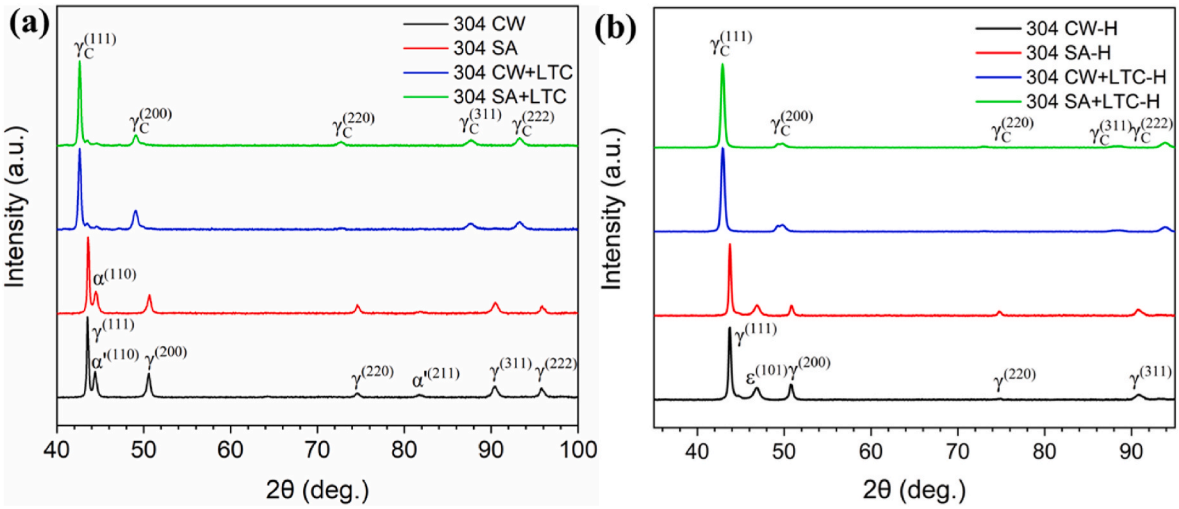

Fig. 3. XRD patterns from the specimens without (a) and with (b) hydrogen uptake. Hydrogen charging was performed at 80 °C for 24 h with a current density of 30 mA/cm^2.

reduction in carbon concentration, confirming that interstitial carbon provides significant solid solution strengthening. Christiansen et al. [24] reported that high surface carbon content caused lattice distortion and compressive stress. In the present study, the higher hardness of 304 CW + LTC relative to 304 SA + LTC can be explained by the combined effects of a high dislocation density introduced by cold drawing and the presence of deformation-induced martensite.

3.2. Phase evolution

To examine the effect of hydrogen uptake on phase constituents, XRD measurements were performed on both uncharged and hydrogen-charged samples, and the results are shown in Fig. 3. For 304 CW, small martensite (α') peaks induced by cold working were observed in addition to the strong austenite (γ) peaks (Fig. 3a). For 304 SA, weaker peaks at the same positions might be introduced by sample preparation. For LTC-treated samples, only diffraction peaks from austenite were present. These peaks appeared broadened and shifted towards lower angles, and the α' peaks nearly disappeared. The peak shift is attributed to lattice expansion due to supersaturated carbon incorporated into γ_c during LTC treatment. The absence of the α' peaks can be explained by recovery phenomena, facilitated by the thermal energy provided by LTC. Previous studies [25,26] have reported that recovery within this temperature range may revert martensite back to austenite.

After hydrogen charging, a significant amount of ε-martensite was observed in both 304 CW-H and 304 SA-H, as seen in Fig. 3b. According to the unary iron phase diagram [27], ε-Fe with a hcp structure forms at a pressure/stress exceeding 13 GPa. It has been reported that electrochemical hydrogen charging introduces large stresses as high as ~110 GPa on the steel surface [28,29]. In addition, hydrogen uptake lowers the stacking fault energy (SFE), further facilitating the γ → ε transformation [30]. The formation of ε-martensite in both 304 CW-H and 304 SA-H is therefore attributed to the combined effects of high internal stress and reduced SFE resulting from hydrogen absorption. In contrast, the LTC samples exhibited little to no martensite transformation after hydrogen uptake, indicating γ_c present in these samples effectively suppresses hydrogen-induced martensitic transformation.

3.3. Hydrogen-induced microstructure modification, strain and cracking

To reveal the effect of hydrogen charging on the microstructure, quasi-in-situ SEM and EBSD studies were performed before and after hydrogen charging at the same location, as shown in Figs. 4–6. Fig. 4a is the secondary electron (SE) image of 304 CW. The grain boundaries and twins could be clearly shown. The phase map in Fig. 4b confirmed that 304 CW was dominated by γ phase with a small amount of α' phase. The orientation of grains and twins can be distinguished in IPF map in Fig. 4c. The gradient color within the grains indicated the local strain caused by cold working. The KAM map in Fig. 4d shows that high strain was located at the grain boundaries. Hydrogen charging at a current density of 1 mA/cm^2 for 1 h at 80 °C probably induced a few microcracks, as marked by black circles in Fig. 4e. Most of them were related to the martensite phase, as referred to the dashed circle in Fig. 4f. Interestingly, α' and ε were mixed, suggesting a possible transformation between them. Koyama et al. [31] reported strain induced transformation from ε to α'. Comparison of Fig. 4c with Fig. 4g revealed that orientation changes of {111} and {101} grains was caused by martensitic phase transformation (refer to Fig. 4f). It seemed that the {001}-oriented grains were more stable in terms of grain orientation. Note that hydrogen uptake led to increased strain, as shown by the high KAM value in Fig. 4h.

For 304 CW + LTC, no martensite was observed in the phase map, as shown in Fig. 5b. However, compared with 304 CW, LTC treatment increased the misorientation (Figs. 4d and 5d). This effect was related to the lattice distortion induced by high carbon concentration in γ_C. Hydrogen charging under the same condition (at 80 °C with the current density of 1 mA/cm^2 for 1 h) did not cause any surface cracking, as shown in the SE image in Fig. 5. This implied an improved HE resistance. The stable γ phase (Fig. 5b) was present after hydrogen charging (Fig. 5f), indicating that LTC treatment inhibited martensitic transformation. Comparing the IPF maps before and after hydrogen charging (Fig. 5c and g), it was found that hydrogen uptake did not change the grain orientation. As seen in the KAM map, hydrogen uptake led to an increase in misorientation, i.e., strain, not only for 304 CW (Fig. 4d and h), but also for 304 CW + LTC (Fig. 5d and h). The synergistic effect of carburizing and hydrogen uptake gave rise to the largest misorientation (Fig. 5h). Interestingly, this local strain was orientation dependent. For instance, the strain levels of grain 1 with {100} orientation and grain 2

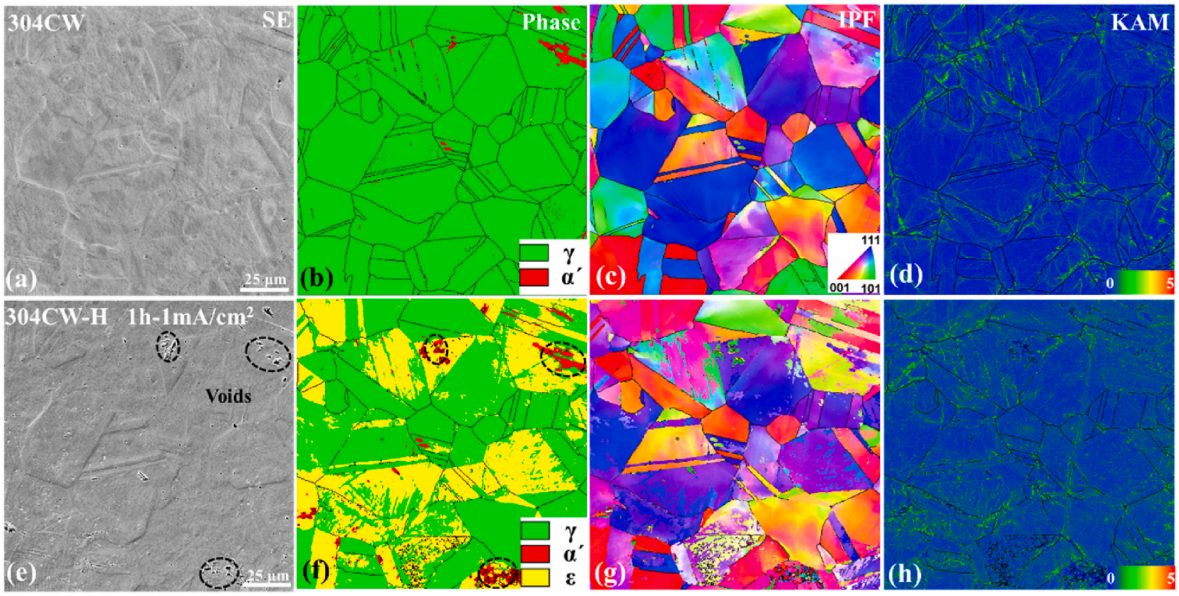

Fig. 4. The quasi-in-situ SEM/EBSD reveals the effect of hydrogen uptake on the microstructure of 304 CW. Hydrogen-charging was performed with 1 mA/cm^2 for 1 h at 80 °C.

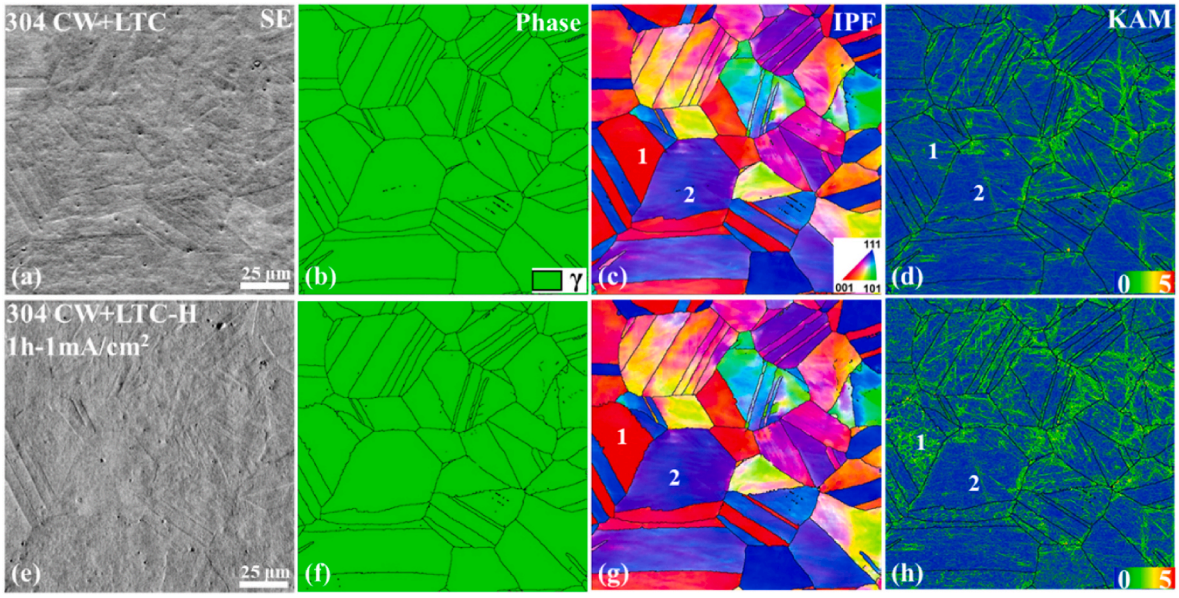

Fig. 5. The quasi-in-situ SEM/EBSD reveals the effect of hydrogen uptake on the microstructure of 304 CW + LTC. Hydrogen-charging was performed at 1 mA/cm^2 for 1 h at 80 °C.

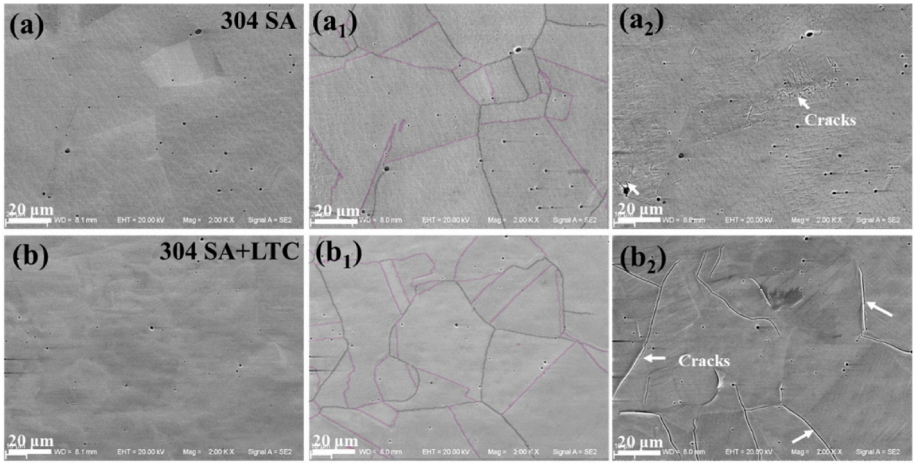

Fig. 6. The quasi-in-situ SEM images reveal the effect of hydrogen uptake on the microstructure of 304 SA (a, a_1 and a_2) and 304 SA + LTC (b, b_1 and b_2). (a) and (b) were hydrogen-free, (a_1) and (b_1) were hydrogen charged for 1 h, (a_2) and (b_2) were charged for 3 h at 80 °C with a current density of 1 mA/cm^2, respectively.

with {111} orientation differed significantly after hydrogen uptake (Fig. 5c–d and g-h). The former one, i.e., grain 1, had a higher strain. This might be related to the high hydrogen diffusion on low-index planes.

For as-received 304 CW, as seen in Fig. 4, hydrogen charging at 80 °C with the current density of 1 mA/cm^2 for 1 h led to a few microcracks, martensitic transformation and increased strain. Although prior LTC treatment increased the microstrain (Fig. 5d vs. Fig. 4d), subsequent hydrogen charging did not induce phase transformation and surface cracking. For instance, the {101}-and {111} oriented grains undergo martensitic transformation in 304 CW-H, while they remain unchanged in 304 CW + LTC-H. Austenite was stabilized with excellent stability by LTC treatment.

As expected, solution annealing increased the resistance to surface cracking due to the annihilation of dislocations induced by cold working. As shown in quasi-in situ SE images of 304 SA in Fig. 6a and a_1, short hydrogen charging for 1 h did not cause obvious microstructural changes and cracks. It was the same for 304 SA + LTC (Fig. 6b and b_1). However, different surface morphologies were observed after 3 h of hydrogen charging. For 304 SA, needle-like microcracks were found in some grains (Fig. 6a_2). For 304 SA + LTC, some long cracks appeared at grain boundaries, as marked by the white arrows (Fig. 6b_2), demonstrating hydrogen uptake may lead to grain boundary cracking. However, no cracking occurred at the twin boundaries, indicating that coincidence site lattice boundaries [32] were more resistant to hydrogen-induced cracking.

Increasing charging time and current density led to more cracking. Fig. 7 shows the surface morphology of the samples with more severe hydrogen uptake (80 °C for 24 h with a current density of 30 mA/cm^2). For cold-worked and solution-annealed samples without LTC, two different types of cracks were randomly distributed on the surface after hydrogen uptake (Fig. 7a and b). The first type, marked by solid white arrows, was straighter, longer and wider. The narrow and less straight cracks (second type) could also be secondary cracks developed from the main straight crack. The density based on crack number (ρ_{nr}) or length (ρ_l) per unit area was estimated using Image-Pro Plus and summarized in Table 2. For the samples without LTC treatment, the crack density in terms of both ρ_{nr} and ρ_l in 304 SA-H was smaller than that in the 304 CW-

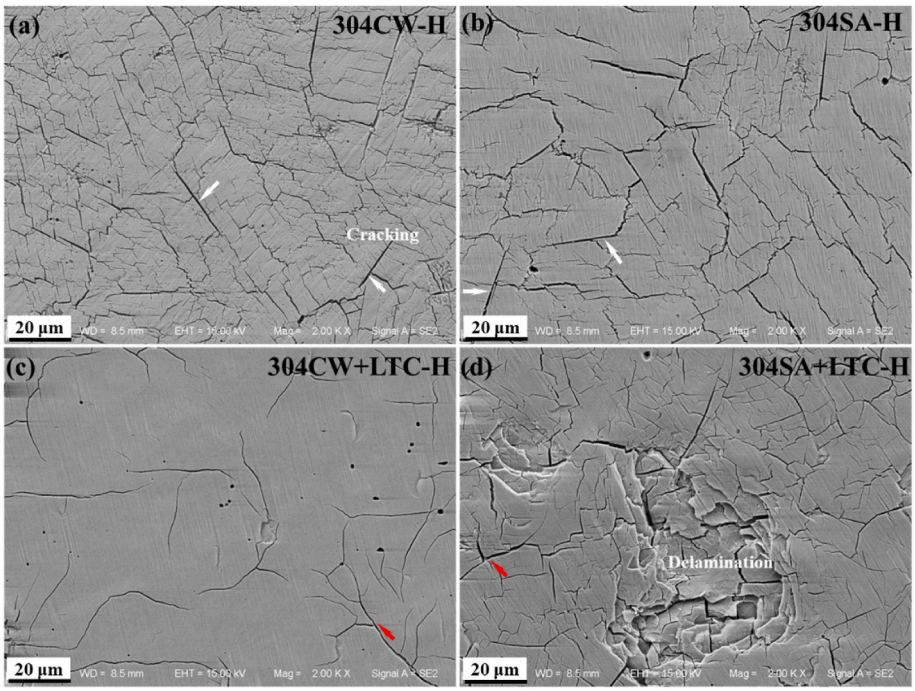

Fig. 7. SEM images of sample surfaces in different conditions after hydrogen charging (a) 304 CW-H, (b) 304 SA-H, (c) 304 CW + LTC-H and (d) 304 SA + LTC-H. Samples were charged at 80 °C for 24 h with a current density of 30 mA/cm^2.

Table 2
Density of cracks in AISI 304 with hydrogen uptake.

Sample	304CW-H	304 -H	304CW + LTC-H	304 + LTC-H
ρ_l (10^4 μm mm^{-2})[a]	8.8	3.5	0.8	4.2
ρ_{nr} (10^5 mm^{-2})[b]	2.8	1.1	0.1	1.1

[a] ρ_l is defined as the length of cracks per unit area.
[b] ρ_{nr} is defined as the number of cracks per unit area.

H. This can be explained by the removal of residual stress and the decrease in defects by solution annealing, as illustrated in Fig. 1b.

Interestingly, the crack density in 304 CW + LTC-H was significantly reduced compared with 304 CW-H (Table 2). The cracks were more tortuous, as marked by the red arrows in Fig. 7c, indicating that LTC treatment changed the crack path in austenite. A tortuous crack path means more energy is consumed. In addition, a few voids were found in 304 CW + LTC-H. This was probably related to the formation of iron and chromium carbides during carburizing [33]. Moreover, smoother surface was present compared to untreated samples, implying higher resistance to hydrogen-induced strain. For 304 SA + LTC-H, delamination and fracture of the expanded austenite were observed (Fig. 7d). Compared with 304 SA-H, 304 SA + LTC-H exhibited the same ρ_{nr} but slightly higher ρ_l (Table 2), implying that the LTC treatment was ineffective in preventing cracking in the solution-annealed condition. However, the cracks in 304 SA + LTC-H were still tortuous, which means more energy was consumed before the crack propagated. The order of cracking tendency induced by hydrogen is 304 CW + LTC <304 SA < 304 SA + LTC <304 CW. Considering cold-worked 304 is often used in industrial applications, the finding in this study has significant technical importance.

To further understand the crack initiation and propagation caused by hydrogen charging, electron channel contrast imaging was performed. Two areas separated by a dashed line in Fig. 8 were examined. The first area (lower part in Fig. 8) was in direct contact with electrolyte (charged

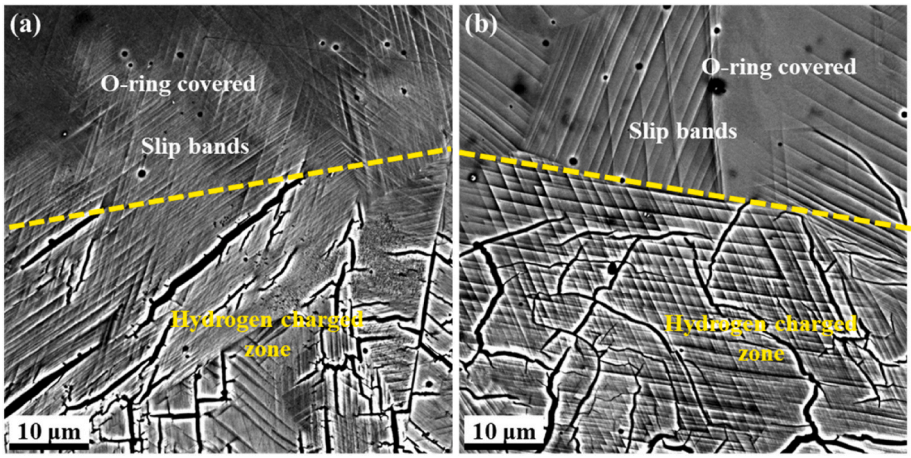

Fig. 8. ECCI images from (a) 304 SA-H and (b) 304 SA + LTC-H. The upper part is the O-ring covered area (H diffusion zone), while the lower part is the hydrogen charged area. Samples were charged at 80 °C for 24 h with a current density of 30 mA/cm^2.

zone), meaning high hydrogen uptake. The second area was covered by an O-ring, but hydrogen could diffuse from the charged zone to this area. Naturally, hydrogen concentration was expected to be lower in this diffusion zone. As shown in Fig. 8, numerous slip bands were observed in both regions on the surface, implying that hydrogen uptake induced plastic deformation. Notice that the samples were polished prior to hydrogen charging. The better contrast in the hydrogen-charged zone is supposed to be related to more plastic deformation due to the higher hydrogen concentration there. Moreover, the hydrogen-charged zone exhibited extensive cracking, while cracking was not observed in the hydrogen diffusion zone. This implied that there might be a critical hydrogen concentration below which cracking would not occur. Another interesting observation was that most straight cracks were along the slip bands in 304 SA-H, as shown in Fig. 8a. For 304 SA + LTC-H, the cracking in the hydrogen-charged area was more tortuous and did not follow the slip bands (Fig. 8b), which meant that LTC changed the path of crack propagation.

3.4. Dislocation observation

Since 304 CW has a higher initial dislocation density, 304 SA was selected to examine the effect of hydrogen uptake on dislocation density. Fig. 9 shows TEM images of 304 SA and 304 SA + LTC before and after hydrogen charging. For 304 SA, few dislocations were observed within the grains except for some isoclinic fringes (Fig. 9a). This was mainly due to the dislocation annihilation promoted by solution annealing. For 304 SA-H, dislocations were observed inside the twin grains, as shown in Fig. 9b. These dislocations were expected to be initiated from high-angle grain boundaries and propagated to twin boundaries. Interestingly, stacking faults were found at twin boundaries. For 304 SA + LTC, some dislocations and stacking faults were also found within the grains (Fig. 9c). It seemed that hydrogen charging led to a significant increase in dislocations for 304 SA + LTC-H, as shown in Fig. 9d. The increase in dislocation density can be related to the increased local strain caused by hydrogen charging, as confirmed by the high KAM values in Figs. 4h & 5h. The findings in this study were consistent with some studies in the literature. Based on the nanoindentation test, Nibur et al. [34] found that dissolved hydrogen reduced the shear stress required for dislocation nucleation in ASS. This also means the dislocation mobility increases. By phase field simulation, Zheng et al. [35] confirmed that hydrogen uptake can promote dislocation nucleation and multiplication in the Frank-Read source, enhancing the hydrogen-induced plasticity.

4. Discussion

This work focuses on the effect of electrochemical cathodic hydrogen charging on the microstructure evolution of LTC 304 ASS. The results show that hydrogen uptake significantly affects the microstructure. The microstructural aspects, such as strain, phases and surface morphology are crucial for understanding the HE mechanism and will be discussed in this section.

4.1. Hydrogen uptake increases strain

The KAM maps in Fig. 4d, h and Fig. 5d, h show that hydrogen charging leads to an increased local strain. Likewise, the slip bands observed in the hydrogen-charged samples in Fig. 8 indicate plastic deformation. Strain generally leads to an increase in dislocation density,

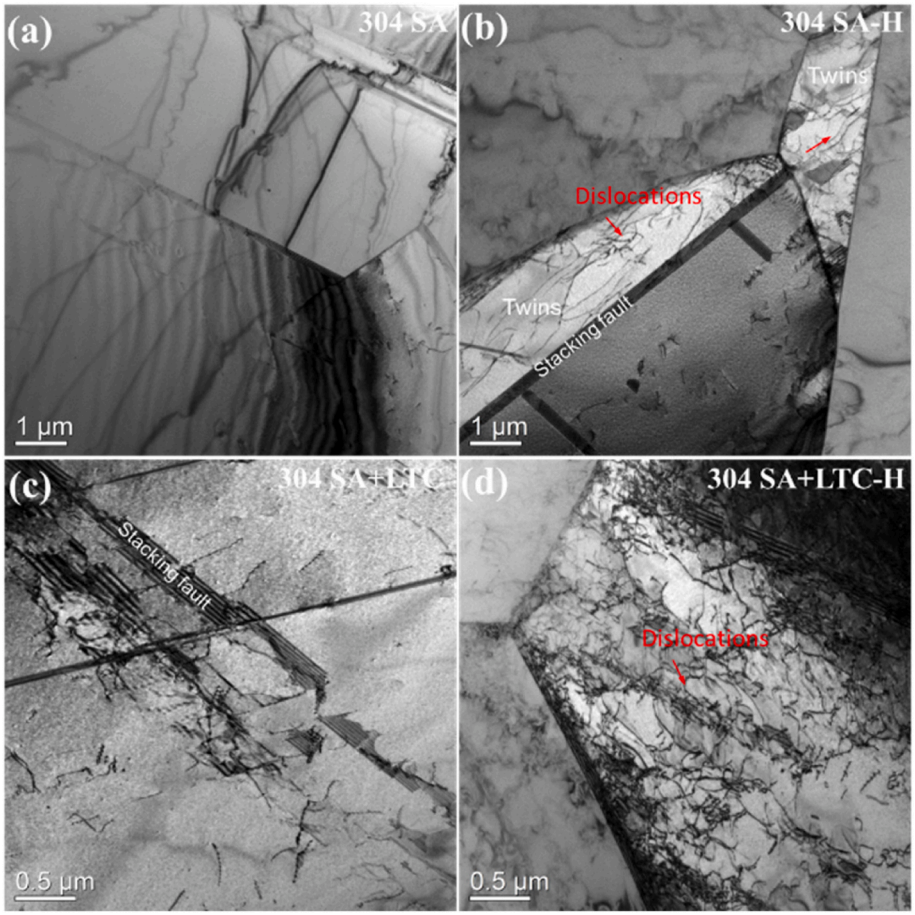

Fig. 9. Low magnification TEM images from hydrogen-free (a and c) and hydrogen-charged specimens (b and d) in solution annealing condition. The samples were hydrogen charged at 80 °C for 24 h with a current density of 30 mA/cm^2.

as confirmed by the TEM images in Fig. 9. The increase in strain during the cathodic hydrogen charging is affected by many factors such as stress, phase transformation, defects and environment.

In this study, the electrolyte, i.e., sulfuric acid solution, acted as an effective hydrogen source in the cathodic charging process. Supersaturation of hydrogen atoms on the steel surface during hydrogen charging induces extremely high stress. Moreover, interstitial hydrogen atoms in the lattice usually lead to lattice distortion. Rozenak [27] calculated that the maximum tensile stress on the surface of the hydrogen-charged sample reached as high as 110 GPa, which was much greater than the yield strength of 304 (~610 MPa and ~200 MPa for cold-worked and solution-annealed 304, respectively). When the stress is higher than the yield strength, plastic deformation occurs. Phase transformation is another important factor for the increase of strain. Hydrogen charging induces the transformation of austenite to martensite, resulting in increase in dislocation densities and strains. Defects such as grain boundaries, phase boundaries, or inclusions can accumulate hydrogen and consequently enhance local plastic deformation, leading to an inhomogeneous strain distribution.

In fact, increased strain is caused by the interaction between dislocations and hydrogen under the stress induced during hydrogen charging. The increase in dislocation density and mobility due to hydrogen uptake has been reported by several researchers [34–40]. Deutges et al. [36] introduced hydrogen into palladium alloy before cold rolling, which led to a significant increase in dislocation density. Defactant mechanism [36,37] believes that the solute hydrogen segregated to defects (such as vacancies, dislocations, grain boundaries, etc.) will reduce dislocation formation energy, leading to an increased dislocation density. Meanwhile, decrease in the interaction energy of dislocations enhances the dislocation mobility. Some other studies claimed that hydrogen increases dislocation mobility by reducing Peierls-Nabarro stress [38], or by elastically shielding or lowering the interaction energy [39] between dislocations and other defects (such as impurities, solute atoms, precipitates, etc.). Tarzimoghadam [40] observed that hydrogen precharging directly promoted strain localization and enhanced the formation of microcracks, leading to shear failure along slip bands. Lynch [41,42] reasoned that the increased strain was due to enhanced dislocation emission from crack tips, caused by hydrogen adsorption on the crack surfaces.

4.2. Low temperature carburizing stabilizes austenite

Austenite stability is an important factor affecting HE. The phase transformation from face-centered cubic austenite (FCC γ) to body-centered cubic (BCC α′) martensite and hexagonal close-packed (HCP ε) phase is associated with changes in hydrogen solubility and/or diffusivity. As shown in Fig. 3a, the deformation induced α′ martensite is observed in 304 CW. The low hydrogen solubility and high hydrogen diffusivity in martensite lead to high susceptibility to HE, which has been widely reported in the literature [14,15]. As the martensite content increases, the susceptibility to HE increases significantly [43]. LTC leads to the formation of expanded austenite with a stable FCC structure, as revealed in Fig. 3a. This makes martensite transformation difficult. It is worth noting that after hydrogen charging, the intensity of α′ martensite peak reduces significantly and ε martensite peak appears from XRD patterns, as shown in Fig. 3b. The EBSD phase map in Fig. 4 also reveals that hydrogen charging leads to martensitic phase transformation and ε martensite is dominant. However, a few newly formed α′ is observed after hydrogen charging. Considering that the information obtained by EBSD is from a small area in the depth of a few nanometers, this is supposed to be a local behavior. Nevertheless, hydrogen charging caused the phase transformation in the as-received 304 sample. The transformation of γ or α′ to ε is related to the extremely high stress introduced by hydrogen charging. Internal stress or strain associated with supersaturated hydrogen uptake may provide an important driving force for austenite transformation/decomposition. The stability of the γ phase is reduced and it transforms into ε and α′-martensite [31]. For the LTC sample, stable austenite is still present after hydrogen charging (Figs. 3b and 5f). Qin et al. [44] introduced an expanded austenite on the surface of cold worked 304 to inhibit hydrogen uptake. It has been found that LTC treated 304 shows a lower hydrogen embrittlement index (HEI) of 10.4 % compared to 304 (HEI = 45.7 %). Jiang et al. [21] also reported that low-temperature carburizing has a positive effect on improving the HE resistance of 304 L.

4.3. Hydrogen charging induces cracking

As described earlier, surface cracking developed on all samples with increasing charging current and time during electrochemical charging. Such phenomena are rarely reported and documented in literature, as most studies emphasize mechanical property changes after hydrogen charging, while modifications in surface morphology due to hydrogen uptake are often overlooked. In this study, the sample surface was mechanically polished before hydrogen charging to minimize surface roughness, enabling direct observation of microstructural changes during cathodic charging. The presence of surface cracks demonstrated that hydrogen uptake alone can cause severe damage. HIC is supposed to be closely related to the hydrogen concentration, stress/strain state in the material, and its microstructural characteristics.

Hydrogen charging in acidic electrolytes results in high hydrogen fugacity. The low hydrogen diffusivity of ASS results in a large concentration gradient of H in the surface region. The internal stress caused by the non-uniform expansion of lattice is one of the important driving forces for crack formation. Regarding LTC, the effect is two-fold. From one side, LTC treatment stabilizes austenite and eliminates martensite transformation, leading to improved cracking resistance. On the other hand, the lattice distortion caused by supersaturated carbon also induces internal stress, making crack formation easier. These two factors compete with each other. Whether LTC is beneficial or not depends on which factor prevails.

As shown in Figs. 7 and 304 CW, 304 SA, 304 CW + LTC, and 304 SA + LTC exhibit different degrees of cracking under the same hydrogen charging conditions. For 304 CW, martensite formation, high-density dislocations, and local high strains make hydrogen accumulate easily at these locations. Consequently, high stress introduced may lead to crack initiation and propagation. Compared with 304 CW, 304 SA with dominant austenite has lower dislocation density and lower strain level. Therefore, less cracking is observed when hydrogen charging under the same condition. LTC improves the austenite stability of 304 CW, inhibiting hydrogen-induced martensitic transformation. This is the governing factor counteracting the brittleness caused by internal stress due to hydrogen and carbon in the investigated steel, leading to the least cracking. For 304 SA + LTC, the expanded austenite is also stabilized. However, it shows a high cracking tendency, as seen in Fig. 7. It has been found in our tensile test that the HEI of 304 SA + LTC was 23.7 %, which was much higher than 304 SA (HEI = 3.4 %). These results suggest that LTC treatment cannot improve the HE resistance of 304 SA.

Despite similar γ_C thickness (~22 μm) on the steel surface, 304 CW + LTC and 304 SA + LTC show opposite behaviors in terms of cracking tendency caused by hydrogen uptake. The crack density in numbers for 304 SA + LTC-H is nearly 10 times more than that of 304 CW + LTC-H (Table 2). Notice the surface carbon concentration of 304 SA + LTC is ~2.5 wt%, which is double compared with 304 CW + LTC (1.25 wt%). It is even higher than the maximum carbon solubility of austenite (2.11 wt % at 1147 °C). Jiang et al. [45] reported that the carbon concentration in a 30 μm-thick γ_C layer reached approximately 2.6 wt%, corresponding to a residual stress as high as - 2.2 GPa at surface. The residual stress decreases with the depth and carbon concentration. The extremely high residual stress can induce premature cracking. Superimposed over the effect of hydrogen uptake, significantly higher internal stress is accompanied by larger lattice distortion and higher dislocation density for 304 SA + LTC-H, making the benefits from austenite stabilization less

important. The consequence is the significantly increased crack density for 304 SA + LTC-H. In addition, 304 SA + LTC-H with high carbon content risks carbide precipitation due to its thermodynamic instability. Carbides can trap more hydrogen, as implied by the higher hydrogen level for 304 SA + LTC-H (18 ppm) compared to 304 SA-H (10.2 ppm). This may also increase the cracking tendency. However, further experimental confirmation is required.

In this study, hydrogen was introduced into the steel by cathodic charging without applying external stress. Nevertheless, cracking occurred on the surface during the charging process. This is a form of environmentally assisted HIC. It is worth noting that the initiation and propagation of cracks depend on hydrogen charging condition including current density, time and temperature, and initial microstructure. These factors in turn determine the level of hydrogen uptake. Hydrogen concentration greatly affects the HE mechanism [8]. As mentioned earlier, the main HE mechanisms include HEDE and HELP. The former one, i.e., HEDE, often works under high hydrogen concentration conditions. For hydrogen charging using high current density, more hydrogen uptake is expected. Hydrogen accumulation at interfaces such as grain boundaries leads to reduced cohesive strength and promotes intergranular cracking. The higher the hydrogen concentration, the more obvious HEDE is, especially in areas with high dislocation density or at boundaries. For HELP mechanism, it occurs more under low hydrogen concentration conditions, such as hydrogen charging using low current density for short time. The characteristic of HELP mechanism is the increased dislocation mobility, which leads to local plastic deformation and transgranular cracking along slip bands. In this study, hydrogen-induced crack propagation is observed at grain boundaries, slip bands and martensite regions, implying a mixture of these two mechanisms. Grain boundary cracking is consistent with HEDE mechanism, while cracking along slip bands agrees with the HELP mechanism. It is worth noting that HELP mechanism may promote hydrogen migration to specific locations, increasing local hydrogen concentration, and thus triggering HEDE. This synergistic effect may lead to complex crack initiation and propagation behaviors.

Electrochemical charging is a simple and effective method to introduce hydrogen into steel. It has been widely used as a charging method to introduce H into material before mechanical testing. It should be mentioned that the cracks formed during charging may affect the subsequent hydrogen diffusion and the mechanical properties [47]. Unfortunately, few researchers have paid attention to this so far. Surface cracking during the electrochemical charging process should be avoided when evaluating the susceptibility to HE. Based on the results of this study, reducing the hydrogen charging current density or time can reduce surface cracking. Attention should also be given to the influence of different hydrogen charging conditions. Variations in electrolytes (e.g., neutral or alkaline) and hydrogen charging methods can affect both hydrogen uptake and the resulting stress state, thereby influencing failure behavior. It has been found that there is no surface cracking during hydrogen charging in neutral or alkaline electrolytes, indicating that the pH value plays a critical role in surface degradation. In acidic environments, the high concentration of H^+ ions promotes greater hydrogen absorption, which induces high surface stress and, consequently, cracking. This aligns with widely reported findings that hydrogen charging in acidic electrolytes leads to more severe hydrogen embrittlement (HE) [46,47]. In contrast, gaseous hydrogen charging is typically conducted under high-temperature and high-pressure conditions to enhance hydrogen uptake and minimize concentration gradients, resulting in a more uniform hydrogen distribution compared to electrochemical methods. Unlike electrochemical charging, gaseous hydrogen charging—dominated by physical adsorption and atomic diffusion—generally does not induce stress-related surface cracking or phase transformations [48].

5. Conclusions

In this work, the effect of cathodic hydrogen charging on the microstructure of low-temperature carburized (LTC) 304 austenitic stainless steel was investigated using SEM, XRD, EBSD and TEM. The main conclusions are summarized as follows.

(1) LTC treatment produced an expanded austenite layer (~22 μm thick) with high carbon content, large strain and lattice distortion, and hardness exceeding 750 HV. Both hardness and C content in γ_C decreased monotonically with the depth.
(2) Hydrogen charging led to increased strain and dislocation density. For untreated 304, hydrogen-induced martensitic transformation was orientation-dependent. LTC treatment stabilized the metastable austenite and effectively suppressed hydrogen-induced martensitic transformation.
(3) Hydrogen charging parameters, including current density, time, and microstructure, strongly influenced surface cracking. Cracks preferentially initiated and propagated along grain boundaries, slip bands and martensite. The hydrogen-induced cracking susceptibility followed the order: 304 CW + LTC <304 SA < 304 SA + LTC <304 CW.
(4) How LTC treatment affected cracking tendency/hydrogen embrittlement of 304 was governed by the competition between enhanced austenite stability and internal stress associated with carbon concentration. For cold worked 304, LTC treatment markedly reduces hydrogen-induced cracking because the stabilization of austenite outweighed the detrimental effect of internal stress. In contrast, for solution annealed 304, the high surface carbon concentration in 304 SA + LTC was the dominant factor, leading to increased cracking.

CRediT authorship contribution statement

Xiao Qin: Writing – original draft, Validation, Methodology, Investigation, Formal analysis, Data curation, Conceptualization. **Lars Nyborg:** Visualization, Validation, Resources, Investigation, Conceptualization. **Huiqun Liu:** Visualization, Validation, Methodology, Investigation. **Alexandra Bauer:** Visualization, Resources, Investigation, Funding acquisition. **Yu Cao:** Writing – review & editing, Visualization, Validation, Supervision, Resources, Project administration, Methodology, Investigation, Funding acquisition, Formal analysis.

Declaration of competing interest

The authors declare that they have no known competing financial interests or personal relationships that could have appeared to influence the work reported in this paper.

Acknowledgments

This work was financed by the competence center TechForH2 hosted by Chalmers University of Technology and financially supported by the Swedish Energy Agency (P2021-90268) and the member companies Volvo, Scania, Siemens Energy, GKN Aerospace, PowerCell, Oxeon, RISE, Stena Rederier AB, Johnson Matthey and Insplorion, Sweden's innovation agency (2021-01908), Production Area of Advance, Chalmers University of Technology, and China Scholarship Council.

References

[1] Acar C, Dincer I. The potential role of hydrogen as a sustainable transportation fuel to combat global warming. Int J Hydrogen Energy 2020;45(5):3396–406.
[2] Dwivedi SK, Vishwakarma M. Hydrogen embrittlement in different materials: a review. Int J Hydrogen Energy 2018;43:21603–16.
[3] Robertson IM, Sofronis P, Nagao A, Martin ML, Wang S, Gross DW, Nygren KE. Hydrogen embrittlement understood. Metall Mater Trans A 2015;46:2323–41.

[4] Lynch S. Hydrogen embrittlement phenomena and mechanisms. Corros Rev 2012;30(3–4):105–23.
[5] Nguyen TT, Heo HM, Park J. Damage assessment and mechanical performance of Cr-Mo steel used in hydrogen storage vessels. Eng Fail Anal 2021;120:105031.
[6] Martin ML, Dadfarnia M, Nagao A. Enumeration of the hydrogen-enhanced localized plasticity mechanism for hydrogen embrittlement in structural materials. Acta Mater 2019;165:734–50.
[7] Birnbaum HK, Petros S. Hydrogen-enhanced localized plasticity-mechanism for hydrogen-related fracture. Mater Sci Eng A 1994;176:191–202.
[8] Wasim M, Djukic MB, Ngo TD. Influence of hydrogen-enhanced plasticity and decohesion mechanisms of hydrogen embrittlement on the fracture resistance of steel. Eng Fail Anal 2021;123:105312.
[9] Wilson BT, Robson JD, Shanthraj P. Simulating intergranular hydrogen enhanced decohesion in aluminium using density functional theory. Model Simul Mater Sci Eng 2022;30(3):035009.
[10] Jemblie L, Olden V, Akselsen OM. A coupled diffusion and cohesive zone modelling approach for numerically assessing hydrogen embrittlement of steel structures. Int J Hydrogen Energy 2017;42(16):11980–95.
[11] Hirata K, Iikubo S, Koyama M. First-principles study on hydrogen diffusivity in BCC, FCC, and HCP iron. Metall Mater Trans A 2018;49:5015–22.
[12] Okayasu M, Fujiwara T. Effects of microstructural characteristics on the hydrogen embrittlement characteristics of austenitic, ferritic, and γ–α duplex stainless steels. Mater Sci Eng A 2021;807:140851.
[13] Rodoni E, Verbeken K, Depover T, Iannuzzi M. Effect of microstructure on the hydrogen embrittlement, diffusion, and uptake of dual-phase low alloy steels with varying ferrite-martensite ratios. Inter J Hydrogen Energy 2024;50:53–65.
[14] Wang Y, Wu X, Wu W. Effect of α′martensite content induced by tensile plastic prestrain on hydrogen transport and hydrogen embrittlement of 304L austenitic stainless steel. Metals 2018;8(9):660.
[15] Rozenak P. Stress induce martensitic transformations in hydrogen embrittlement of austenitic stainless steels. Metal Mater Trans A 2014;45:162–78.
[16] Zhang H, Zheng L, Wang T. Interrelationship between hydrogen and α′-martensite of SUS 304 austenitic stainless steel revealed by tensile tests. Mater Sci Eng A 2022;831:142169.
[17] Michal GM, Ernst F, Kahn H, Cao Y, Oba F, Agarwal N, Heuer AH. Carbon supersaturation due to paraequilibrium carburization: stainless steels with greatly improved mechanical properties. Acta Mater 2006;54:1597–606.
[18] Sun Y, Li X, Bell T. Structural characteristics of low temperature plasma carburised austenitic stainless steel. Mater Sci Technol 1999;15:1171–8.
[19] Borgioli F. From austenitic stainless steel to expanded austenite-S phase: formation, characteristics and properties of an elusive metastable phase. Metals 2020;10:187.
[20] Sun Y, Li X, Bell T. Low temperature plasma carburising of austenitic stainless steels for improved wear and corrosion resistance. Surf Eng 1999;15(1):49–54.
[21] Jiang Y, Wu Q, Wang Y, Zhao J, Gong J. Suppression of hydrogen absorption into 304L austenitic stainless steel by surface low temperature gas carburizing treatment. Int J Hydrogen Energy 2019;44:24054–64.
[22] Li Y, Li W, Zhu X, Zhou H, Jin X. Mechanism of improved hydrogen embrittlement resistance of low-temperature plasma carburised stainless steel. Surf Eng 2018;34(3):189–92.
[23] Rey O, Jacquot P. Kolsterising: hardening of austenitic stainless steel. Surf Eng 2002;18:412–4.
[24] Christiansen TL, Somers MAJ. Stress and composition of carbon stabilized expanded austenite on stainless steel. Metal Mater Trans A 2009;4:1791–8.
[25] Takahashi T, Bassett WA. High-pressure polymorph of iron. Science 1964;145:483–6.
[26] Panov D, Kudryavtsev E, Chernichenko R, Smirnov A, Stepanov N, Simonov Y, Salishchev G. Mechanisms of the reverse martensite-to-austenite transformation in a metastable austenitic stainless steel. Metals 2021;11(4):599.
[27] Yang DP, Wu D, Yi HL. Reverse transformation from martensite into austenite in a medium-Mn steel. Scripta Mater 2019;161:1–5.
[28] Zhang T, Chu WY, Gao KW, Qiao LJ. Study of correlation between hydrogen-induced stress and hydrogen embrittlement. Mater Sci Eng A 2003;347:291–9.
[29] Rozenak P, Loew A. Stress distributions due to hydrogen concentrations in electrochemically charged and aged austenitic stainless steel. Corros Sci 2008;50(11):3021–30.
[30] Hermida JD, Roviglione A. Stacking fault energy decrease in austenitic stainless steels induced by hydrogen pairs formation. Scr Mater 1998;39(8):1145–9.
[31] Koyama M, Okazaki S, Sawaguchi T, Tsuzaki K. Hydrogen embrittlement susceptibility of Fe-Mn binary alloys with high Mn content: effects of stable and metastable ε-martensite, and Mn concentration. Metall Mater Trans A 2016;47:2656–73.
[32] Seita M, Hanson JP, Gradečak S, Demkowicz MJ. The dual role of coherent twin boundaries in hydrogen embrittlement. Nat Commun 2015;6(1):6164.
[33] Maistro G, Yao Y, Klement U, Nyborg L, Cao Y. On surface carbides in low-temperature carburized austenitic stainless steels. Mater Charact 2020;167:110462.
[34] Nibur KA, Bahr DF, Somerday BP. Hydrogen effects on dislocation activity in austenitic stainless steel. Acta Mater 2006;54:2677–84.
[35] Zheng Z, Liang S, Huang M, Zhao L, Zhu Y, Li Z. Studying the effects of hydrogen on dislocation mobility and multiplication in nickel by phase-field method. Mech Mater 2022;173:104443.
[36] Deutges M, Barth HP, Chen Y. Hydrogen diffusivities as a measure of relative dislocation densities in palladium and increase of the density by plastic deformation in the presence of dissolved hydrogen. Acta Mater 2015;82:266–74.
[37] Kirchheim R. On the solute-defect interaction in the framework of a defactant concept. Int J Mater Res 2009;100(4):483–7.
[38] Zheng Z, Liang S, Zhu Y, Huang M, Li Z. Studying hydrogen effect on the core structure and mobility of dislocation in nickel by atomistically-informed generalized Peierls–Nabarro model. Mech Mater 2020;140:103221.
[39] Yu P, Cui Y, Zhu GZ, Shen Y, Wen M. The key role played by dislocation core radius and energy in hydrogen interaction with dislocations. Acta Mater 2020;185:518–27.
[40] Tarzimoghadam Z, Ponge D, Klöwer J, Raabe D. Hydrogen-assisted failure in Ni-based superalloy 718 studied under in situ hydrogen charging: the role of localized deformation in crack propagation. Acta Mater 2017;128:365–74.
[41] Lynch SP. Environmentally assisted cracking: Overview of evidence for an adsorption-induced localised-slip process. Acta Metall 1988;36(10):2639–61.
[42] Lynch SP. A fractographic study of hydrogen-assisted cracking and liquid-metal embrittlement in nickel. J Mater Sci 1986;21:692–704.
[43] Wang Y, Wu X, Li X, Wu W, Gong J. Combined effects of prior plastic deformation and sensitization on hydrogen embrittlement of 304 austenitic stainless steel. Int J Hydrogen Energy 2019;44(13):7014–31.
[44] Qin X, Nyborg L, Liu H, Bauer A, Cao Y. Low-temperature carburizing improves hydrogen embrittlement resistance of cold worked 304 austenitic stainless steel. J Mater Res Tech 2025;36:8816–25.
[45] Jiang Y, Li Y, Peng Y, Gong J. Mechanical properties and cracking behavior of low-temperature gaseous carburized austenitic stainless steel. Surf Coat Tech 2020;403:126343.
[46] Zhang P, Laleh M, Hughes AE, Marceau RK, Hilditch T, Tan MY. A systematic study on the influence of electrochemical charging conditions on the hydrogen embrittlement behaviour of a pipeline steel. Int J Hydrogen Energy 2023;48(43):16501–16.
[47] Lu X, Wang D, Wan D, Zhang ZB, Kheradmand N, Barnoush A. Effect of electrochemical charging on the hydrogen embrittlement susceptibility of alloy 718. Acta Mater 2019;179:36–48.
[48] Yun HS, Jeon SK, Lee YK, Park JS, Nahm SH. Effect of precharging methods on the hydrogen embrittlement of 304 stainless steel. Int J Hydrogen Energy 2024;50:175–88.